Applied Physics Letters

Topotactic transformation in $SrFeO_{3-\delta}$ triggered by low-dose Ga^+ focused ion irradiation

Cite as: Appl. Phys. Lett. **116**, 163103 (2020); https://doi.org/10.1063/1.5141154
Submitted: 04 December 2019 . Accepted: 05 April 2020 . Published Online: 20 April 2020

Elías Ferreiro-Vila, David Bugallo, César Magén, Francisco Rivadulla, and José María De Teresa

Applied Physics Letters ARTICLE scitation.org/journal/apl

Topotactic transformation in $SrFeO_{3-\delta}$ triggered by low-dose Ga^+ focused ion irradiation

Cite as: Appl. Phys. Lett. **116**, 163103 (2020); doi: 10.1063/1.5141154
Submitted: 4 December 2019 · Accepted: 5 April 2020 ·
Published Online: 20 April 2020

Elías Ferreiro-Vila,[1,a] David Bugallo,[1] César Magén,[2,3,4] Francisco Rivadulla,[1] and José María De Teresa[2,3,4,a]

AFFILIATIONS

[1]Centro de Investigación en Química Biolóxica e Materiais Moleculares (CIQUS), Departamento de Química-Física, Universidade de Santiago de Compostela, 15782 Santiago de Compostela, Spain
[2]Instituto de Ciencia de Materiales de Aragón (ICMA), CSIC-Universidad de Zaragoza, 50009 Zaragoza, Spain
[3]Departamento de Física de la Materia Condensada, Universidad de Zaragoza, 50009 Zaragoza, Spain
[4]Laboratorio de Microscopías Avanzadas (LMA), Instituto de Nanociencia de Aragón (INA), Universidad de Zaragoza, 50018 Zaragoza, Spain

[a]Authors to whom correspondence should be addressed: elias.ferreiro.vila@gmail.com and deteresa@unizar.es

ABSTRACT

We introduce a single-step lithography process based on Ga^+-focused ion beam (FIB) irradiation to trigger a topotactic transformation on $SrFeO_{3-\delta}$ thin films, from the perovskite to the brownmillerite (BM) crystal structure. The crystallographic transformation is triggered by preferential oxygen sputtering by Ga^+-FIB irradiation, which favors the formation of the $SrFeO_{2.5}$ BM phase. The transformation has been verified through micro-Raman spectroscopy on thin films subjected to Ga^+-FIB irradiation under 5 kV and 30 kV. Inducing crystallographic transformations by FIB in a single-step process (without the need of resists), at a very high speed (low Ga^+ doses are required, in the range of 10^{15} ions/cm^2), with very high spatial resolution (limited by the ion beam spot, of a few square nanometers) and with potential for upscaling using broad Ga^+ beams, this approach represents a significant forward step over previous methods using multistep lithographic or electrochemical procedures. All these virtues make this process appealing to develop applications based not only on $SrFeO_{3-\delta}$ thin films but also on other oxide films harnessing topotactic transformations.

Oxoperovskites (PV) $(Ca,Sr)(Fe,Co)O_{3-\delta}$ exhibit fast O^{2-}-ion mobility and electrical conductivity at high temperature. Thus, PV thin films of $Fe^{3+/4+}$ and $Co^{3+/4+}$ can be fully reduced to the 3+ brownmillerite (BM) structure upon high-temperature annealing under vacuum or by mild reduction with CaH_2.[1–10] The crystallographic transformation occurs by topotactic oxygen exchange and can be made reversible by annealing the BM in air or oxygen at moderate temperatures. This combination makes oxygen-deficient PV very appealing for the development of memory devices,[10] solid oxide fuel cells,[11,12] batteries, or oxygen separation membranes.[13,14]

The very high oxygen-vacancy mobility in $SrFeO_x$ also made possible the electric field-driven topotactic phase transformations (TPts) using electrochemical cells[10,15–20] and voltage-biased AFM tips,[21] which allows control down to the micrometer-size scale. However, the time required for the transformation (of several minutes for a small micrometer-size pattern) and the spatial resolution must be improved to develop competitive devices. Importantly, Ar^+ beam etching on $SrTiO_3$ was found to produce preferential etching, giving rise to the creation of oxygen vacancies.[22–24] It is, thus, tempting to propose that an ion-beam-based process can potentially induce a TPt PV-to-BM transformation in $SrFeO_{3-\delta}$, with a significant advantage toward an enhancement in the process speed and the scalability, which are required for applications.

The focused ion beam (FIB) is a matured nanopatterning technique exploiting the use of an ion beam that is finely focused (<10 nm) on the surface of a material.[25] Main FIB-based applications are nanoscale milling and deposition, which are named FIB-milling and FIBID (focused ion beam induced deposition), respectively.[26] Both techniques are pivotal for important technological processes such as circuit edit,[27] mask repair,[28] lamellae preparation,[29] device prototyping,[30] and the growth of singular functional materials.[31] In addition, FIB irradiation can be applied for resist-based focused ion beam lithography,[32] modification of etching properties of Si-based materials,[33] controlled creation of defects,[34] the growth of carbon

nanomembranes,[35] modification of 2D materials,[36] cryo-FIBID,[37] modification of magnetic properties (anisotropy,[38] exchange,[39] and domain wall velocity[40]), fabrication of high-T_C superconducting devices,[41] etc. Moreover, broad-beam ion irradiation can be combined with masks containing microscale or nanoscale holes in order to obtain micro-patterns or nanopatterns with high throughput.[42]

The present work was devised following the hypothesis that Ga^+-FIB irradiation could trigger a topotactic PV-to-BM transformation on $SrFeO_{3-\delta}$ thin films. As sketched in Fig. 1, the underlying idea was the potential effect of FIB irradiation to remove O atoms selectively from the original PV $SrFeO_{3-\delta}$ film, producing the transformation of the irradiated areas into the BM $SrFeO_{2.5}$ phase. This is a physical effect brought in by the high ion energy, which, in the present work, ranges from 5 keV to 30 keV. As the ion irradiation removes a substantial amount of O atoms by preferential sputtering, the perovskite film lowers its energy through its transformation into the brownmillerite $SrFeO_{2.5}$ phase, which is the most stable one when the local concentration of oxygen vacancies is large enough. This is conceptually different from previous works, which focused on the use of local electric fields[21] or low-energy plasmas[43] to achieve topotactic transformations in this oxide. Moreover, our proposed strategy is a single-step lithography process that does not require resists, it allows high-resolution nanopatterning, and it can be scaled to large areas if the required ion dose to induce the topotactic transformation is low (as shown hereafter).

A Ga^+-FIB column forming part of Dual Beam Helios equipment (from Thermo Fisher Scientific) has been used for these experiments. Using 30 kV ion acceleration, the resolution of this column is 4.5 nm, which can be attained using low ion currents (a few pA). In order to investigate the dependence of the observed effects with the ion energy, experiments have been carried out under 30 keV and 5 keV. The low current used, 13.8 pA under 30 kV and 15 pA under 5 kV, warrants a high lateral resolution of the process, especially under 30 kV, voltage at which the equipment exhibits the best resolution due to the minimization of the lens aberrations. As shown in the supplementary material, the average milling rate has been found to be 0.18 μm^3/nC under 30 kV and 0.15 μm^3/nC under 5 kV. An irradiated area of 24 μm^2 with 13.8 pA under 30 kV is expected to decrease its thickness ≈1 nm after 10 s.

Several areas of 4×6 μm^2 of PV $SrFeO_{3-\delta}$ were irradiated with a varying dose of Ga^+ ions accelerated at 5 kV and 30 kV. Under 5 kV, the minimum and maximum ion irradiation times used in the experiments were 0.1 s and 100 s, corresponding to areal doses of 3.9×10^{13} ions/cm^2 (= 6.24 μC/cm^2) and 3.9×10^{16} ions/cm^2 (= 6240 μC/cm^2), respectively. Under 30 kV, the minimum and maximum ion irradiation times used in the experiments were 0.2 s and 100 s, corresponding to areal doses of 7.19×10^{13} ions/cm^2 (= 11.5 μC/cm^2) and 3.59×10^{16} ions/cm^2 (= 5750 μC/cm^2), respectively. As shown in the SEM micrographs of Fig. 2, the irradiated areas show a change in contrast with respect to the pristine film. The origin of this change in contrast is a combination of different factors, but the most straightforward explanation is the different electrical conductivity between the PV (semiconducting) and the BM (wide-bandgap semiconducting) phases. The decrease in the local electrical conductivity after ion irradiation has been verified by means of electrical measurements using conductive-probe AFM (CP-AFM), shown in Fig. 2(d) and in the supplementary material (Fig. S2).

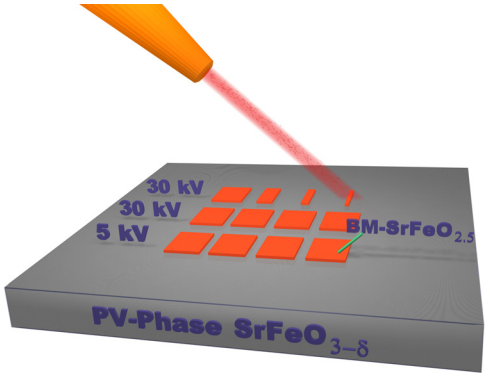

FIG. 1. Conceptual sketch of the experiment: under Ga^+-FIB irradiation, the $SrFeO_{3-\delta}$ films, originally in the PV phase, will transform into the $SrFeO_{2.5}$ BM phase. Technical details on the thin-film growth can be found in the supplementary material. The 4×6 μm^2 rectangles have been irradiated for various ion doses using ion beam voltages of 5 kV and 30 kV. The experiments on high-resolution irradiation down to a lateral size of 10 nm have been carried out using an ion beam voltage of 30 kV.

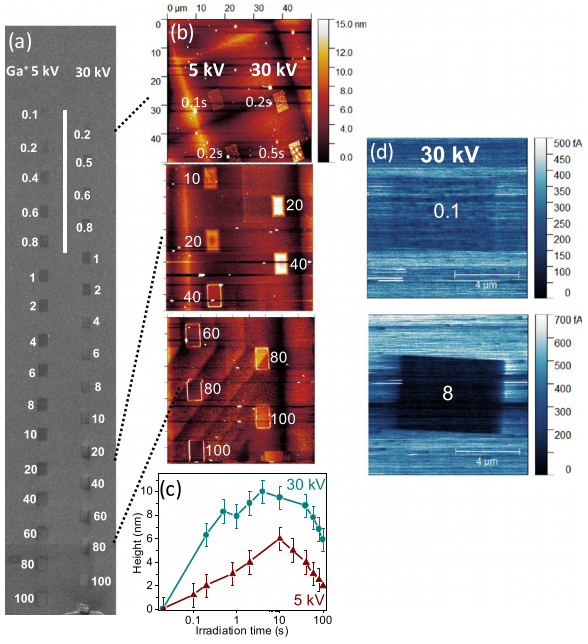

FIG. 2. (a) SEM image and (b) AFM topography of the PV $SrFeO_{3-\delta}$ thin film after several rectangles (4×6 μm^2) have been patterned with a Ga^+ FIB irradiation at different doses (expressed in seconds) for 5 kV (left column) and 30 kV (right column) ions. The white line in the SEM micrograph corresponds to a 100 μm scale bar. All the AFM images have an area of 50×50 μm^2 and include the same color scale for topography. (c) Surface expansion of the corresponding structures as a function of the irradiation time. (d) Local electrical conductance probed by conductive-probe AFM. The irradiated portions of the film become electrically more insulating as the Ga^+ dose increases, producing the flow of lower electrical current. See the main text for the correspondence between the irradiation time and the irradiation dose (in ions/cm^2 and μC/cm^2). Technical details of the AFM equipment used can be found in the supplementary material.

AFM topography reveals a substantial expansion of the film thickness on the irradiated areas, which can be as high as 10 nm (20% of the initial film thickness), as shown in Fig. 2(c). Different tips (conductive and insulating) with different force constants were employed in different scanning modes (contact and non-contact) to discard any possible artifact from electromechanical coupling during the topography measurements. The larger pseudocubic lattice parameter of the BM phase compared to the PV cannot be explained by the magnitude of the expansion. A similar effect was reported after the application of large local electric fields with an AFM tip,[21] as well as in electrochemically modified $SrCoO_{2.5}$.[10] In these cases, the introduction of H into the BM phase was invoked to explain this large expansion of the cell. In this case, insertion of Ga^+ ions is a plausible hypothesis, given that low-dose Ga^+ irradiation can promote swelling.[44]

Figure 2(c) shows that the use of 30 kV Ga^+ irradiation produces a larger local expansion than 5 kV due to the different penetration length of 5 kV and 30 kV Ga^+ ions in the film. Simulations with the SRIM (the stopping and range of ions in matter) code indicate that the ion range for 30 kV Ga^+ ions in a $SrFeO_3$ film is 30 nm, whereas it decreases to 10 nm for 5 kV Ga^+ ions. Thus, under 30 kV Ga^+ irradiation, the PV-to-BM transformation is expected to occur only at 30 nm close to the film surface and, under 5 kV Ga^+ irradiation, only at 10 nm close to the film surface. On top of this transformation, the ion irradiation will also produce milling, which explains the decrease in the film thickness under high irradiation doses (typically above 40 s).

Figure 3 shows the variation, as a function of the irradiation dose, of the Raman spectra of the same irradiated rectangles shown in Fig. 2(a). The appearance of the Raman peaks at ≈230 cm^{-1}, 331 cm^{-1}, ≈430 cm^{-1}, and ≈625 cm^{-1} in the unirradiated regions of the film is the characteristic of a tetragonal or orthorhombic PV phase and composition $SrFeO_x$, with x ≈ 2.7–2.9.[45] The intensity of these peaks decreases gradually with the Ga^+ irradiation time, and, simultaneously, a broad maximum with a shoulder at ≈710 cm^{-1}, characteristic of the stretching modes of FeO_4 tetrahedra in the BM phase, appears.[46] Thus, the results shown in Fig. 3 confirm that the Ga^+ irradiation provokes the transformation of the PV phase into the BM one. Also, there is a relationship between the progressive transformation observed in the Raman spectra and the thickness expansions measured by AFM and shown in Fig. 2(c).

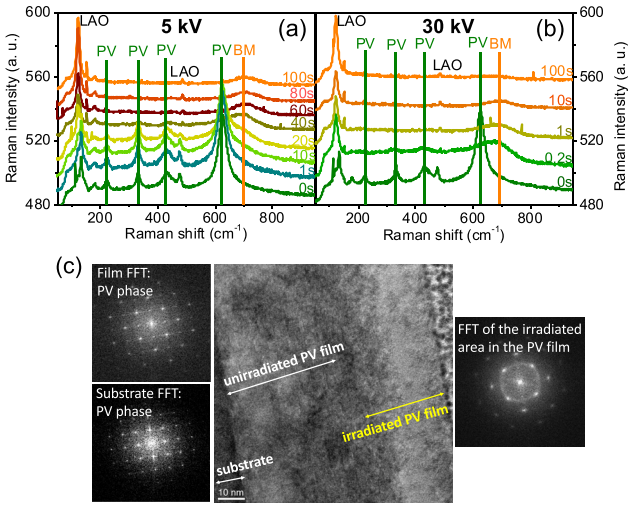

FIG. 3. (a) Room-temperature Raman spectra ($\lambda = 532.19$ nm) of the PV film after 5 kV Ga^+-FIB irradiation over different regions with an increasing dose (time of irradiation). (b) The same for 30 kV Ga^+-FIB irradiation. The spectra were displaced vertically for the sake of clarity. The Raman peaks produced by the $LaAlO_3$ (LAO) substrate (120 and 480 cm^{-1}) are indicated. The peaks characteristic of the PV and BM phases are pinpointed by vertical dashed lines. It can be noticed that the peak at ≈700 cm^{-1}, which is characteristic of the BM phase, comes up as the ion irradiation dose increases. (c) High-resolution cross-sectional TEM image of a film area with an on-purpose 25.7 $\mu C/cm^2$ (or 0.4 s) irradiation dose under 30 kV Ga^+. The FFT images of the LAO substrate, the underlying unirradiated PV film, and the irradiated top part of the film are also shown. Technical details of the Raman equipment used and additional TEM results can be found in the supplementary material.

Besides, the results shown in Figs. 2 and 3 indicate that the use of 30 kV Ga^+ irradiation is more efficient than the use of 5 kV owing to the larger penetration range of Ga^+ in the film under 30 kV (30 nm vs 10 nm). As a consequence, for the same irradiation dose, the measured thickness expansion is smaller for 5 kV, and the Raman spectra show a mixture of peaks corresponding to the PV and BM phases. Moreover, the Raman spectra of the areas irradiated at the highest doses exhibit an intensity decrease and broadening of the BM peak, suggesting the milling and the amorphization of the crystal structure, in agreement with the AFM data. Both phenomena, the PV-to-BM phase transformation induced by low-dose Ga^+ irradiation and the amorphization effect under high-dose Ga^+ irradiation, are consistent with the Transmission Electron Microscopy (TEM) results, shown in Fig. 3(c) and in the supplementary material (Figs. S3 and S4). TEM experiments in these samples are difficult, given that the unknown amount of Ga^+ irradiation during the lamella preparation generally induces the PV-to-BM transformation in the pristine film. However, in the selected example shown in Fig. 3(c), the pristine film still retains the PV phase after the lamella preparation, whereas a change in the crystallographic structure is observed in the top 30 nm due to the on-purpose 30 kV Ga^+ irradiation. From the fast Fourier transform (FFT) of this area, it is not possible to determine its exact crystallographic structure, possibly due to the disorder effect and grain disorientation produced by the on-purpose Ga^+ irradiation plus the unwanted Ga^+ irradiation during the lamella preparation. The amorphization effect under high-dose Ga^+ irradiation is clearly observed in the images included in the supplementary material (Fig. S4).

Moreover, annealing experiments have been carried out to verify that the PV-to-BM phase transformation induced by low-dose Ga^+ irradiation is reversible. The topography and electrical measurements carried out by AFM confirm the reversibility of this phenomenon, as discussed in the supplementary material and shown in Fig. S5.

From all these experiments, we conclude that an optimized process for the PV-to-BM transformation should make use of a suitable ion energy for a given film thickness (30 kV for a film thickness of 30 nm) and privilege low doses (in the range of 10^{14} ions/cm^2) in order to minimize the processing time and the potential amorphization effects. This is a remarkable result, given that the process speed is significantly enhanced compared to other methods,[21] and comparable to some of the fastest nanopatterning processes existing nowadays.[47]

Another advantage of FIB technology is its potential for high-resolution nanopatterning. In order to investigate the lateral resolution of the PV-to-BM transformation by means of Ga^+ focused irradiation, we have chosen 30 kV irradiation with a dose of 5.1×10^{15} ions/cm^2, which is maintained for rectangles in which one side is still 6 μm, but

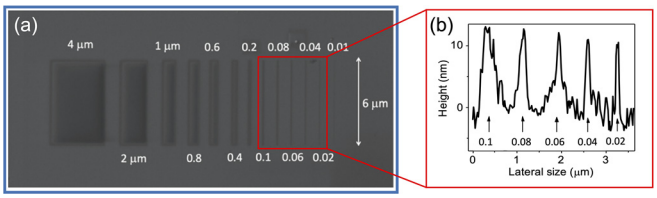

FIG. 4. (a) SEM micrograph of the PV film after 30 kV Ga^+-FIB irradiation with a dose of 5.1 × 10^{15} ions/cm^2 over different regions with a constant vertical (Y) dimension of 6 μm and varying horizontal (X) dimensions, ranging from 4 μm down to 10 nm. (b) AFM topographic measurements of the height of the irradiated areas with X dimensions from 100 nm down to 20 nm.

the second side is progressively reduced from 4 μm down to 10 nm. As shown in Fig. 4(a), a neat change in contrast can be noticed in the SEM micrographs, which corresponds to the irradiated areas with a rectangular shape, in which one side shrinks progressively. AFM measurements have been performed on the irradiated areas to investigate the change in the height produced by the ion irradiation. According to the obtained results, shown in Fig. 4(b), all the investigated rectangles showed an expansion, as expected for the PV-to-BM transformation. We were able to measure the expansion even for the rectangle with a lateral size of 20 nm. Although the precise expansion profile for these tiny irradiations cannot be obtained from these measurements due to the convolution with the large AFM tip, the sharp contrast observed in the SEM micrographs suggests that the process resolution is of the order of the ion beam spot.

In summary, low-dose Ga^+-30 kV-FIB irradiation has been found to induce a topotactic transformation in $SrFeO_{3-\delta}$ films, originally in the PV phase and converting into the $SrFeO_{2.5}$ BM phase due to preferential oxygen sputtering. The method offers significant advantages in terms of speed, simplicity, and high spatial resolution. Moreover, the method could be applicable to other oxide materials undergoing similar topotactic transformations and scalable to large areas by the combination of broad Ga^+ beams with pierced masks. Our results open the route to the future design of nanodevices using preferential ion etching to produce different functionalities in oxides.

See the supplementary file for the equipment description, milling rate experiments, conductive-probe AFM measurements, TEM results, and investigation of annealing treatments.

This work was supported by the Spanish Ministry of Economy and Competitivity through Project Nos. MAT2017-82970-C2-2-R, MAT2018-102627-T, and MAT2016-80762-R (including FEDER funds), by the Aragon Regional Government through Project No. E13_20R (with European Social Fund), by Xunta de Galicia (Centro singular de investigación de Galicia accreditation 2016–2019, No. ED431G/09), and by the European Union (European Regional Development Fund-ERDF) and the European Commission through the Horizon H2020 funding by H2020-MSCA-RISE-2016-Project No. 734187–SPICOLOST. D.B. acknowledges financial support from Ministerio de Ciencia e Investigación (Spain) through an FPI fellowship (No. BES-2017-079688). We are grateful to Pablo Orús for performing the simulations on the Ga^+ penetration length using the SRIM code, to Victor Leborán for help in drawing Fig. 1, to Lucía Iglesias for help in the AFM measurements, to the RIAIDT-USC Raman facilities, and to Isabel Rivas, Mariano Barrado and Laura Casado from the LMA for experimental help during the FIB irradiation and lamellae preparation.

REFERENCES

[1]W. Paulus, C. Tassel, M. Ceretti, M. Takano, T. Watanabe, H. Kageyama, Y. Tsujimoto, C. Ritter, N. Hayashi, and K. Yoshimura, Nature **450**, 1062 (2007).
[2]S. Inoue, M. Kawai, N. Ichikawa, H. Kageyama, W. Paulus, and Y. Shimakawa, Nat. Chem. **2**, 213 (2010).
[3]W. S. Choi, T. S. Yoo, M. Kim, J. Lee, T. D. Kang, D. Shin, A. Khare, T. W. Noh, H. Ohta, J. Hwang, S. W. Kim, I.-H. Jung, and S. Roh, Adv. Mater. **29**, 1606566 (2017).
[4]Y. Shimakawa, Bull. Chem. Soc. Jpn. **86**, 299 (2013).
[5]H. Yamada, M. Kawasaki, and Y. Tokura, Appl. Phys. Lett. **80**, 622 (2002).
[6]C. Tassel and H. Kageyama, Chem. Soc. Rev. **41**, 2025 (2012).
[7]H. Jeen, W. S. Choi, J. W. Freeland, H. Ohta, C. U. Jung, and H. N. Lee, Adv. Mater. **25**, 3651 (2013).
[8]A. Khare, J. Lee, J. Park, G. Y. Kim, S. Y. Choi, T. Katase, S. Roh, T. S. Yoo, J. Hwang, H. Ohta, J. Son, and W. S. Choi, ACS Appl. Mater. Interfaces **10**, 4831 (2018).
[9]S. Roh, S. Lee, M. Lee, Y. S. Seo, A. Khare, T. Yoo, S. Woo, W. S. Choi, J. Hwang, A. Glamazda, and K. Y. Choi, Phys. Rev. B **97**, 075104 (2018).
[10]N. Lu, P. Zhang, Q. Zhang, R. Qiao, Q. He, H.-B. Li, Y. Wang, J. Guo, D. Zhang, Z. Duan, Z. Li, M. Wang, S. Yang, M. Yan, E. Arenholz, S. Zhou, W. Yang, L. Gu, C.-W. Nan, J. Wu, Y. Tokura, and P. Yu, Nature **546**, 124 (2017).
[11]A. Chroneos, B. Yildiz, A. Taranc, D. Parfitt, and J. A. Kilner, Energy Environ. Sci. **4**, 2774 (2011).
[12]A. J. Fernández-Ropero, J. M. Porras-Vázquez, A. Cabeza, P. R. Slater, D. Marrero-López, and E. R. Losilla, J. Power Sources **249**, 405 (2014).
[13]J. F. Vente, S. McIntosh, W. G. Haije, and H. J. M. Bouwmeester, J. Solid State Electrochem. **10**, 581 (2006).
[14]J. F. Vente, W. G. Haije, and Z. S. Rak, J. Membr. Sci. **276**, 178 (2006).
[15]Q. Lu, Y. Chen, H. Bluhm, and B. Yildiz, J. Phys. Chem. C **120**, 24148 (2016).
[16]Q. Lu and B. Yildiz, Nano Lett. **16**, 1186 (2016).
[17]J. Lee, E. Ahn, Y.-S. Seo, Y. Kim, T.-Y. Jeon, J. Cho, I. Lee, and H. Jeen, Phys. Rev. Appl. **10**, 54035 (2018).
[18]S. Hu and J. Seidel, Nanotechnology **27**, 325301 (2016).
[19]X. Zhong, T. Ma, B. Cui, Y. Zhuang, J. M. Taylor, S. S. P. Parkin, P. Werner, and Z. Wang, Nat. Commun. **9**, 3055 (2018).
[20]A. Maity, R. Dutta, B. Penkala, M. Ceretti, A. Letrouit-Lebranchu, D. Chernyshov, A. Perichon, A. Piovano, A. Bossak, M. Meven, and W. Paulus, J. Phys. D **48**, 504004 (2015).
[21]E. Ferreiro-Vila, S. Blanco-Canosa, I. Lucas del Pozo, H. B. Vasili, C. Magén, A. Ibarra, J. Rubio-Zuazo, G. R. Castro, L. Morellón, and F. Rivadulla, Adv. Funct. Mater. **29**, 1901984 (2019).
[22]D. W. Reagor and V. Y. Butko, Nat. Mater. **4**, 593 (2005).
[23]D. Kan, T. Terashima, R. Kanda, A. Masuno, K. Tanaka, S. Chu, H. Kan, A. Ishizumi, Y. Kanemitsu, Y. Shimakawa, and M. Takano, Nat. Mater. **4**, 816 (2005).
[24]F. Y. Bruno, J. Tornos, M. Gutierrez Del Olmo, G. Sanchez Santolino, N. M. Nemes, M. Garcia-Hernandez, B. Mendez, J. Piqueras, G. Antorrena, L. Morellón, J. M. De Teresa, M. Clement, E. Iborra, C. Leon, and J. Santamaria, Phys. Rev. B **83**, 245120 (2011).
[25]A. A. Tseng, Small **1**, 924 (2005).
[26]L. Bruchhaus, P. Mazarov, L. Bischoff, J. Gierak, A. D. Wieck, and H. Hövel, Appl. Phys. Rev. **4**, 011302 (2017).
[27]Y. Drezner, D. Fishman, Y. Greenzweig, and A. Raveh, J. Vac. Sci. Technol., B **29**, 011026 (2011).
[28]A. Yasaka, F. Aramaki, T. Kozakai, and O. Matsuda, Hitachi Rev. **65**, 71 (2016).
[29]L. A. Giannuzzi and F. A. Stevie, Micron **30**, 197 (1999).
[30]S. Reyntjens and R. Puers, J. Micromech. Microeng. **11**, 287 (2001).
[31]E. S. Sadki, S. Ooi, and K. Hirata, Appl. Phys. Lett. **85**, 6206 (2004).
[32]M. A. Hartney, J. Vac. Sci. Technol., B **9**, 3432 (1991).

[33]G. Rius, J. Llobet, X. Borrisé, N. Mestres, A. Retolaza, S. Merino, and F. Perez-Murano, J. Vac. Sci. Technol., B **27**, 2691 (2009).
[34]A. V. Krasheninnikov and K. Nordlund, J. Appl. Phys. **107**, 071301 (2010).
[35]X. Zhang, H. Vieker, A. Beyer, and A. Gölzhäuser, Beilstein J. Nanotechnol. **5**, 188 (2014).
[36]Z. Li and F. Chen, Appl. Phys. Rev. **4**, 011103 (2017).
[37]R. Córdoba, P. Orús, S. Strohauer, T. E. Torres, and J. M. De Teresa, Sci. Rep. **9**, 14076 (2019).
[38]C. Chappert, H. Bernas, J. Ferre, V. Kottler, and J. Jamet, Science **280**, 1919 (1998).
[39]J. Fassbender and J. McCord, J. Magn. Magn. Mater. **320**, 579 (2008).
[40]L. Serrano-Ramón, A. Fernández-Pacheco, R. Córdoba, C. Magén, L. A. Rodríguez, D. Petit, R. P. Cowburn, M. R. Ibarra, and J. M. De Teresa, Nanotechnology **24**, 345703 (2013).
[41]S. A. Cybart, E. Y. Cho, T. J. Wong, B. H. Wehlin, M. K. Ma, C. Huynh, and R. C. Dynes, Nat. Nanotechnol. **10**, 598 (2015).
[42]E. Menéndez, M. O. Liedke, J. Fassbender, T. Gemming, A. Weber, L. J. Heyderman, K. V. Rao, S. C. Deevi, S. Suriñach, M. D. Baró, J. Sort, and J. Nogués, Small **5**, 229 (2008).
[43]B. M. Lefler, T. Duchoň, G. Karapetrov, J. Wang, C. M. Schneider, and S. J. May, Phys. Rev. Mater. **3**, 073802 (2019).
[44]J. B. Wang, A. Datta, and Y. L. Wang, Appl. Surf. Sci. **135**, 129 (1998).
[45]P. Adler, A. Lebon, V. Damljanović, C. Ulrich, C. Bernhard, A. V. Boris, A. Maljuk, C. T. Lin, and B. Keimer, Phys. Rev. B **73**, 094451 (2006).
[46]M. A. Islam, Y. Xie, M. D. Scafetta, S. J. May, and J. E. Spanier, J. Phys. Condens. Matter **27**, 155401 (2015).
[47]J. M. De Teresa, P. Orús, R. Córdoba, and P. Philipp, Micromachines **10**, 799 (2019).